Heterogeneous Distribution of Dynamic Stress Drop and Relative Fault Strength Recovered from the Results of Waveform Inversion: the 1984 Morgan Hill, California, Earthquake

AUTHOR(S):

Mikumo, Takeshi; Miyatake, Takashi

Bulletin of the Seismological Society of America, Vol. 85, No. 1, pp. 178–193, February 1995

Heterogeneous Distribution of Dynamic Stress Drop and Relative Fault Strength Recovered from the Results of Waveform Inversion: the 1984 Morgan Hill, California, Earthquake

by Takeshi Mikumo[1] and Takashi Miyatake

Abstract The dynamic rupture process of the 1984 Morgan Hill, California, earthquake (M = 6.2) has been investigated on the basis of a three-dimensional (3D) dynamic shear crack model, from previous waveform inversion results. For this purpose, a locking fracture criterion is introduced for rupture propagation, from which a lower bound of the peak shear stress just before rupturing, and hence of the relative fault strength, has been estimated at each fault segment. The distribution of static and dynamic stress drops has also been independently evaluated from that of fault slips by linear and nonlinear inversion procedures, respectively.

The results show that large slips located from the hypocenter to about 10 km and 14 to 17 km along the strike at depths between 8 and 12 km result from local dynamic stress drops exceeding 40 and 140 bars, respectively. Negative stress drops down to −15 bars are required to explain very low slips over a shallow fault section. If a non-negative stress-drop condition is imposed, somewhat larger slips are obtained there than those from the waveform inversion. The above results suggest that there could be a zone of velocity-strengthening frictional behavior in the shallow crust, which may have arrested slip motion during rupture propagation. The strength excess is found to be generally small but somewhat larger at a small zone that has delayed rupture propagation. The dynamic rupture initiated from a small nucleus zone with a low stress drop, propagated southeastward, breaking the deeper fault section with high stress drop, and then broke a relatively high strength zone after a short time of arrest, with highest stress drop.

Introduction

Much progress has been attained over the last decade in elucidating the complexities of the source processes of large to moderate-size earthquakes, from both theoretical and observational perspectives. Waveform inversion techniques have been applied to near-source strong motions (Olson and Apsel, 1982; Hartzell and Heaton, 1983, 1986; Spudich and Frazier, 1984; Fukuyama and Irikura, 1986; Takeo, 1987, 1988; Takeo and Mikami, 1987, 1990; Beroza and Spudich, 1988; Mendoza and Hartzell, 1988, 1989; Hartzell, 1989; Hartzell and Iida, 1990; Wald *et al.*, 1990, 1991; Fukuyama, 1991a, b; Steidl *et al.*, 1991, Zeng *et al.*, 1993), as well as to teleseismic body waves (Kikuchi and Kanamori, 1982, 1991; Kikuchi and Fukao, 1985; Das and Kostrov, 1990; Hartzell *et al.*, 1991), and revealed heterogeneous fault-slip or moment-release distribution and sometimes incoherent rupture propagation. It has been suggested, on the other hand, from theoretical and numerical approaches based on spontaneous, dynamic shear-crack models (e.g., Andrews, 1976; Das and Aki, 1977; Mikumo and Miyatake, 1978; Miyatake, 1980; Das, 1981; Day, 1982; Virieux and Madariaga, 1982; Boatwright and Quin, 1986), that these complexities may be attributed mainly to heterogeneous shear stress distributed over the fault and nonuniform fault strength and partly to lateral inhomogeneities of the crustal structure around the fault zones (Mikumo *et al.*, 1987).

Quite recently, a few attempts have been made to compare the results from waveform inversion based on kinematic fault models with those calculated from the dynamic rupture models (Mikumo *et al.*, 1987; Quin,

[1]Present address: Instituto de Geofisica, Universidad Nacional Autonoma de México, Mexico 04510 D.F., Mexico.

1990). It is now required not only from a seismological but also from a tectonic point of view that a more direct approach be taken to convert the spatial distribution of fault slip and the rupture starting times derived from the waveform inversion into the distribution of dynamic stress drop and fault strength. Several studies along this line have been made recently (Miyatake, 1992a, b; Mikumo and Miyatake, 1993; Fukuyama and Mikumo, 1993), and provided significant results. These studies include slightly different approaches, which will be described and compared in a later section.

The main purpose of the present study is to derive the dynamic stress drop and relative fault strength over an extremely heterogeneous fault, by applying the techniques along the above line. The earthquake selected is the 1984 Morgan Hill, California, earthquake, for which high-quality strong motions have been recorded at near-source stations, and complete waveform inversions have been performed (Hartzell and Heaton, 1986; Beroza and Spudich, 1988). Our results will be discussed in detail to check the validity of the solutions in view of realistic tectonic environments.

The Morgan Hill, California, Earthquake

The 24 April 1984 Morgan Hill earthquake (M = 6.2) took place on the Calaveras fault near the junction with the Hayward fault about 17 km east of San Jose, California (37°18.56′ N, 120°40.68′ W) at a depth of approximately 8.5 km (Cockerham and Eaton, 1987). The aftershocks were distributed along and 2 to 3 km east off the Calaveras fault, extending from 5 km to the northeast to approximately 25 km southeast of the epicenter, as reproduced in Figure 1 (Bakun *et al.*, 1984; Cockerham and Eaton, 1987). The distribution with respect to the location of the mainshock epicenter suggests that the rupture of the mainshock propagated primarily southeastward over the fault dipping approximately at 85° to the northeast (Cockerham and Eaton, 1987). The aftershock zone is located just northwest of that of the 6 August 1979 Coyote Lake earthquake (M = 5.9), which ruptured from the epicenter toward the southeast (Liu and Helmberger, 1983).

During the Morgan Hill earthquake, strong ground motions were well recorded at several near-source stations (Shakal *et al.*, 1984; Brady *et al.*, 1984). The Coyote Lake Dam station (CLD), located at the southeast end of the aftershock zone, recorded a peak acceleration of 1.3 g and peak velocity of 79 cm/sec on the horizontal component N285°E (Hartzell and Heaton, 1986; Beroza and Spudich, 1988). Some of the strong-motion records, which indicate the component of ground velocity nearly perpendicular to the fault strike (Hartzell and Heaton, 1986), are reproduced in Figure 2, together with the locations of the Calaveras fault zone and the near-source stations. The records show large-amplitude SH-type motions at Halls Valley (HAL), CLD, and at stations of the Gilroy array, particularly at GI6. It is natural that the perpendicular components had the largest amplitude for a shallow strike-slip earthquake on the Calaveras fault (Hartzell and Heaton, 1986). Somewhat large amplitudes recorded on other components at a few stations may be attributed to lateral heterogeneity in the upper crustal structure (Hartzell and Heaton, 1986; Beroza and Spudich, 1988).

The crustal structure around the Calaveras fault has been obtained from two sources. Figure 3 shows the P-wave velocity structure along the southern section of the fault based on seismic refraction profiling (Bluming *et al.*, 1985) as well as the structure derived for the Livermore section of the fault located farther to the north (Ellsworth and Marks, 1980). The two profiles are essentially similar to each other, although the latter one has sharper velocity contrasts. To compute the crustal response to a point source, i.e., theoretical Green's function, Hartzell and Heaton (1986) used a velocity structure (solid line) similar to the latter, while Beroza and Spudich (1988) used a structure having no velocity discontinuities and reversals.

Previous Results of Waveform Inversion

The fault rupture behavior of the 1984 Morgan Hill earthquake has been recovered in two different wave-

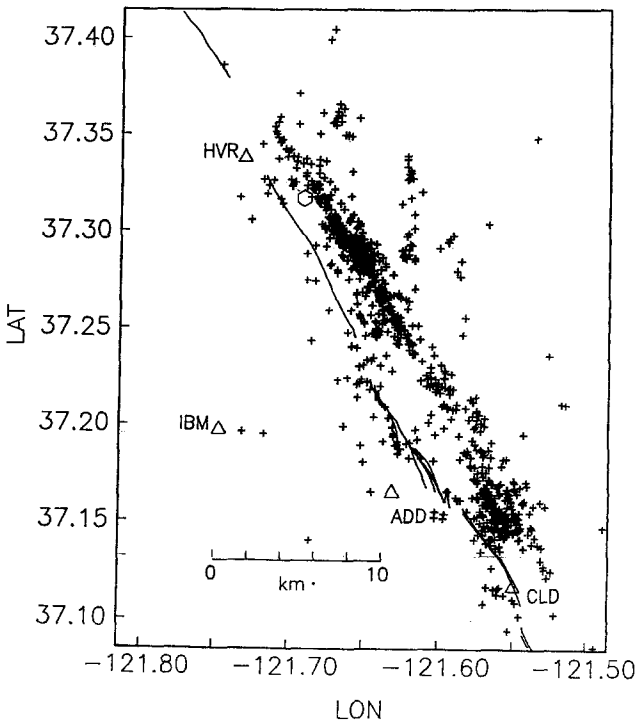

Figure 1. Aftershock distribution of the 1984 Morgan Hill earthquake and the surface trace of the Calaveras fault. The mainshock hypocenter is identified by the hexagon (after Beroza and Spudich, 1988).

form inversions, mainly of strong-motion records. Hartzell and Heaton (1986) used three-component velocity records in the frequency range between 0.2 and 2 Hz at five near-source stations (HAL, CLD, AND, IBM, and GI6), together with teleseismic short-period vertical *P* waveforms recorded at four GDSN stations for forward modeling and an estimate for the overall distribution of slip. The data used by Beroza and Spudich (1988) are the two horizontal-component displacement records obtained at the five nearby stations (HVR, CLD, ADD, IBM, and G06) and the vertical component of the BKS ultra-long-period seismograms. (Notations for the HVR, ADD, and G06 stations in the latter indicate the same stations given by HAL, AND, and GI6 in the former, respectively).

The waveform inversion technique adopted by Hartzell and Heaton (1986) was a constrained, damped least-squares procedure. They assumed a triangular slip-velocity function of 0.3-sec duration, allowing slips in three time windows, with a constant rupture velocity of nine-tenths of the local *S*-wave velocity. Their final model, which yields best-fitting waveforms to the observed records, shows the existence of two high-slip zones, each with an extent of about 5 km along the strike. One slip zone is located near the hypocenter and the other near the center of the fault, separated by about 12 km (Fig. 16 in Hartzell and Heaton, 1986). The maximum slip and the total seismic moment in their model are about 100 cm and 2.1×10^{25} dyne cm, respectively. It should be mentioned, however, that a large second pulse arriving about 10 sec after the onset on the HAL records is not explained by this model.

Beroza and Spudich (1988), on the other hand, performed a linearized inversion of the strong-motion data to recover the distribution not only of slip intensity but also of rupture starting time on the fault. This is more realistic because rupture propagation could be nonuniform on a heterogeneous fault under inhomogeneous stress field, as suggested from dynamic shear-crack models. It has also been suggested (e.g., Yoshida, 1986; Beroza

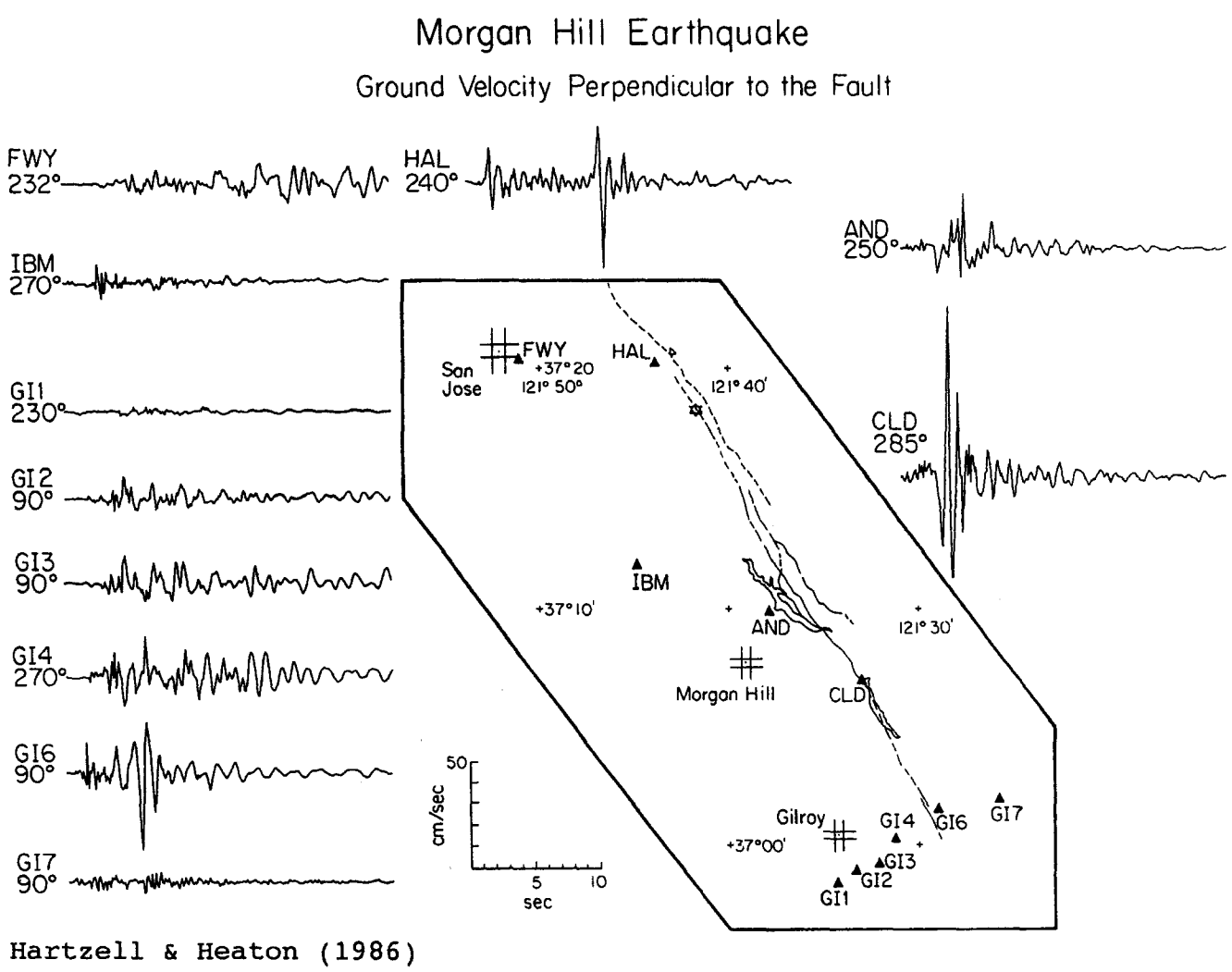

Figure 2. Strong-motion velocity components perpendicular to the Calaveras fault zone, recorded at nearby stations (after Hartzell and Heaton, 1986).

and Spudich, 1988) that slip distribution may not be correctly recovered if one assumes a constant rupture velocity, since the rupture time has a strongly nonlinear dependence on the observed waveforms. Beroza and Spudich solved the nonlinear inverse problem by iteratively perturbing an assumed initial model. The slip-rate source function assumed in their model had a truncated inverse square-root time dependence with a rise time of 0.2 sec, constant everywhere on the fault.

For the above reasons, we refer to the "variable slip—variable rupture velocity model" by Beroza and Spudich (1988) for our discussion. Figure 4 shows their best-fitting model, which indicates the rupture times (in seconds) in the upper diagram and the slip amplitudes (in centimeters) in the lower figure. The fit to the deconvolved displacement waveforms is shown in Figure 5. Note that the large second pulse observed in the *Y* component at HVR (HAL) can be well reproduced by the corresponding synthetic seismogram, although there remains some discrepancy in the *X* component at CLD and in the *Y* component at BKS. The final model indicates extremely heterogeneous slip distribution, including a high-slip zone extending from the hypocenter to about 10 km along the strike at depths between 6 and 12 km, and also a small zone with a maximum slip exceeding 180 cm located at 14 to 17 km along the strike at 8 to 12-km depth. These high-slip zones have also been identified by Hartzell and Heaton (1986), although their locations extended for only 5 km along the strike and the slip amplitudes are somewhat smaller than those in the above model. In contrast, there is a zone of very low slip at depths shallower than 6 km over a wide region of the fault, but the zone of low slip at depth surrounding the high-slip zones might be a result of poor resolution (Beroza and Spudich, 1988). It also appears that the rupture propagation is delayed at 5.25 sec and jumps ahead temporarily leaving a small area behind at approximately 14 km to the southeast of the hypocenter. The average rupture velocity is about 0.8 times the shear-wave velocity, and the seismic moment is found to be 2.7×10^{25} dyne cm in their final model.

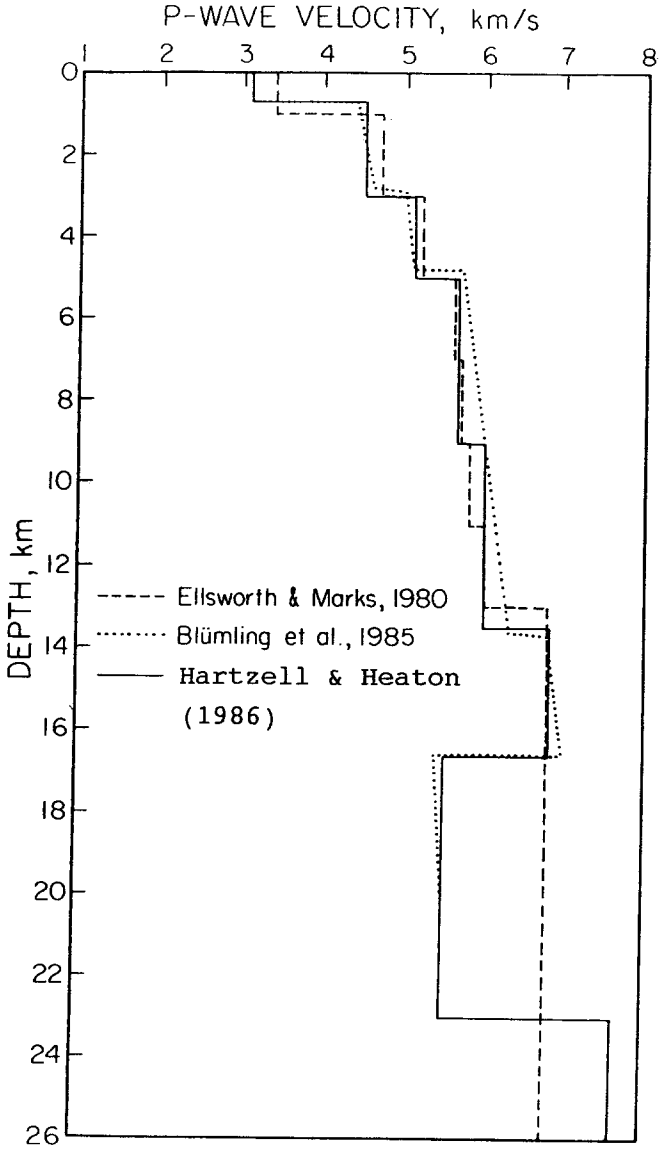

Figure 3. *P*-wave velocity structure for the Calaveras fault region (after Hartzell and Heaton, 1986).

Inversion from Kinematic Fault Model to Dynamic Rupture Model

Now, we attempt to derive the spatial distribution of dynamic stress drop and relative fault strength from the distribution of fault slip and rupture times obtained from the previous waveform inversion, in order to recover the dynamic fault rupture process of the Morgan Hill earthquake. The approach taken here is essentially the same as in Miyatake (1992a, b) and Mikumo and Miyatake (1993), which is summarized below.

Dynamic Rupture Model

The first step is to construct a dynamic rupture model, incorporating kinematic fault parameters estimated by Beroza and Spudich (1988). The fault plane is assumed to be vertical, embedded in a horizontally layered crustal structure, having dimensions of 30 km along the strike and 10 km at depths between 2 and 12 km. The parameters specifying the structure are given in Table 1, which is essentially the same as the crustal model of Hartzell and Heaton (1986) shown in Figure 3, but lacks an uppermost sedimentary layer above 1 km and a low-velocity layer between 17 and 23 km.

The dynamic rupture propagating over the vertical fault can be calculated numerically by solving the wave equation in the 3D space, with appropriate boundary conditions and under a fracture criterion (Mikumo *et al.*, 1987). The boundary conditions imposed here are (1)

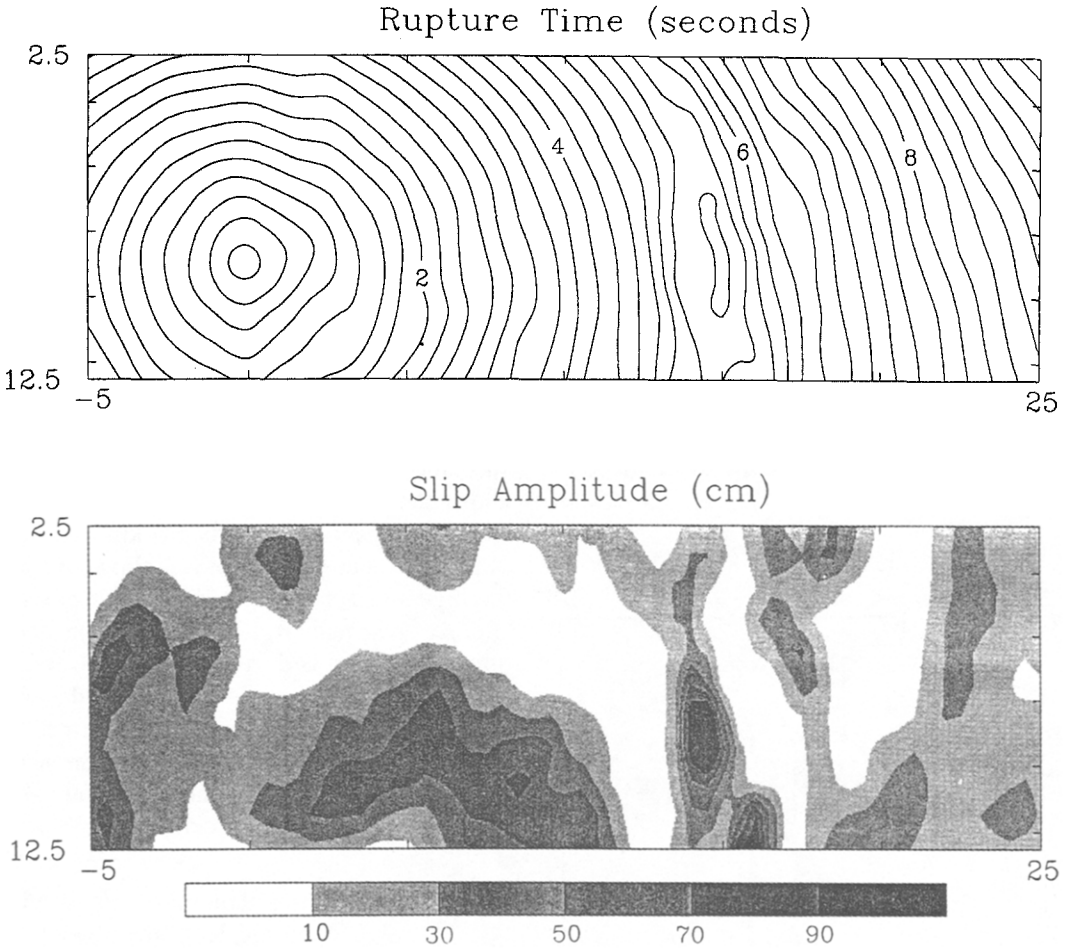

Figure 4. Distribution of the rupture times (*upper*) and the fault slips (*lower*) derived from the linearized inversion in the best-fitting model (after Beroza and Spudich, 1988).

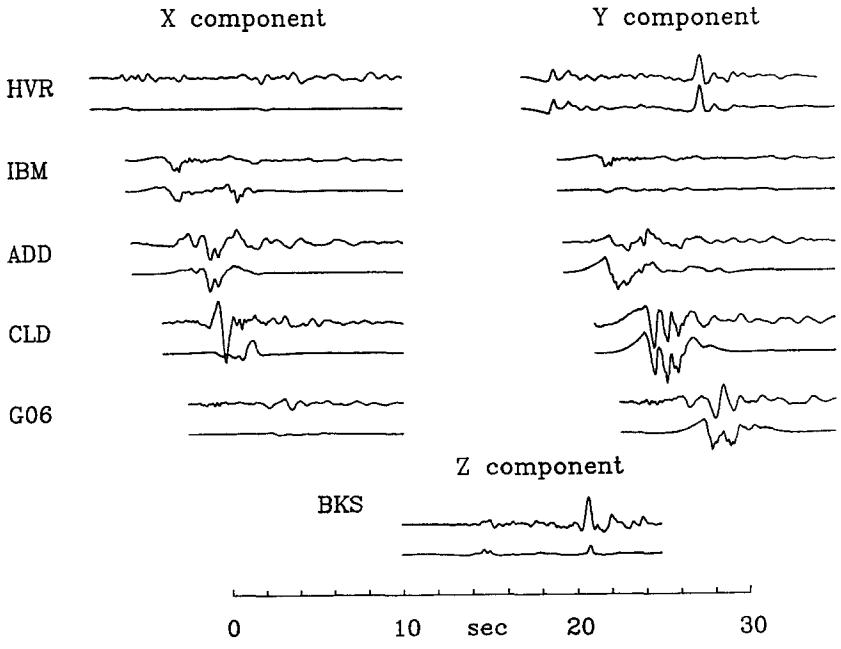

Figure 5. The deconvolved ground displacements and the corresponding synthetic seismograms (after Beroza and Spudich, 1988). Upper traces for each station are the displacements, and the lower traces are the corresponding synthetics.

drop of the initial shear stress to the level of dynamic frictional stress on the fault at the time of rupture arrival, and the continuity of normal stress and normal displacement components across the fault, (2) stress free on the ground surface, (3) the continuity of all stress and displacement components at each of the layer interfaces, and (4) absorbing conditions to attenuate reflected waves at bottom and side boundaries of the model space (Mikumo *et al.* 1987). The grid spacing in the finite-difference scheme is taken to be 1 km, and the time increment is taken as 0.05 sec, so as to satisfy the stability conditions for the 3D wave equations. The initial shear stress, sliding frictional stress, and frictional strength are tentatively taken as 200, 180, and 202 bars, respectively, which gives a uniform stress drop of 20 bars and a uniform strength excess of 2 bars in a starting model. It should be mentioned that in dynamic models, the pattern of rupture propagation and slip distribution is completely governed by dynamic stress drop (the difference between the initial shear stress and the sliding frictional stress) and by strength excess (the difference between the static frictional strength and the initial shear stress) but not by the absolute levels of the three stresses. The above starting values do not affect the estimates of actual dynamic stress drop and strength excess as understood from the inversion procedure described below.

Estimate of the Peak Shear Stress and Strength Excess

For dynamic rupture propagation, we introduce a sort of locking fracture criterion, under which the rupture at each grid point remains locked until the time specified by the waveform inversion. The shear stress at this point continues to increase because of the approach of the rupture front and then drops at this time to the level of dynamic frictional stress. We assume that the peak shear stress just before rupturing this point may be regarded as a good indication of the relative fault strength there (Miyatake, 1992a; Mikumo and Miyatake, 1993). The strength excess is defined here as the difference between the estimated peak shear stress and the assumed initial stress. It is to be mentioned, however, that the value estimated in this way is dependent on the grid spacing and the time increment used in the numerical calculations. These two numerical configurations have to be chosen as small as possible as described above, but the estimated strength excess should still be regarded as a lower bound of its real value. The spatial distribution of their relative values is more important.

Table 1
Parameters Specifying the Crustal Structure

V_p (km/sec)	V_s (km/sec)	(gm · cm^{-3})	H (km)
4.50	2.60	2.45	3.0
5.10	2.94	2.55	2.0
5.65	3.26	2.65	4.0
6.00	3.46	2.70	5.0
6.80	3.92	2.82	9.0
7.60	4.38	2.90	

Estimate of Dynamic Stress Drop

Once the rupture times are specified in dynamic rupture propagation, fault slip at each grid point is roughly linearly related to dynamic stress drop there, although there remain some nonlinear effects received from slips at adjacent fault segments. We apply two different techniques to estimate dynamic stress drop from the fault slip obtained from the waveform inversion.

The first and straightforward approach is to derive static stress drop at each grid point directly from the final fault slips just around there, by solving static equilibrium equations in the 3D space, (Miyatake, 1992a) combined with the boundary conditions described in the Dynamic Rupture Model Subsection. The equilibrium equations to be solved are such that the space derivatives of all stress tensors should be zero, and are solved successively by a finite-difference scheme. This is a linear inverse problem. In this case, a non-negative stress-drop condition can be imposed if we assume that negative stress drop is unlikely to occur over a significant portion of the fault that slipped. However, the validity of this assumption is still open to question. The stress drop estimated in the above way is actually local static stress drop and should be somewhat different from dynamic stress drop during rupture propagation. Considering that there could be overshooting of fault slip, the obtained static stress drop will be adjusted to 90% of its calculated value and taken as dynamic stress drop to calculate dynamic rupture propagation (Miyatake, 1992a, b).

The second, alternative, approach is to apply an iterative least-squares technique (Mikumo and Miyatake, 1993). First, we calculate the distribution of dynamic slips from a starting model with a uniform strength and sliding frictional stress under a homogeneous stress field. We compare the calculated dynamic slips with the kinematic fault slips obtained from the waveform inversion, on each of the subdivided fault segments. The ratio between the kinematic and dynamic slips is multiplied to the initially assumed stress drop in the second iteration, and the distribution of dynamic slips is again calculated in the refined model. This iteration procedure is repeated several times to minimize the square sum of the difference between the kinematic and dynamic fault slips all over the fault within a reasonably small value. The dynamic stress drop will thus be obtained from a best-fitting model. This procedure is actually a nonlinear inversion. Under these procedures, the uncertainties in the kinematic slip affect almost linearly the estimates of the dynamic stress drop.

Dynamic Rupture Process under Heterogeneous Dynamic Stress Drop and Strength Excess

In this section, we provide the results for the distribution of dynamic stress drop and strength excess, which have been obtained by the two different inversion techniques described previously.

Static Stress Drop

Figure 6 shows the distribution of static stress drop directly inverted from the fault slips based on the best-fitting model of Beroza and Spudich (1988). We immediately notice that locally high static stress drop exceeding 150 bars in the deeper sections of the fault corresponds to high slips around there, and that there is a zone of negative stress drops down to −15 bars corresponding to very low slip in the shallower fault section. The negative stress zone surrounding the high-stress-drop zones extends down to the deeper section of the fault. The above results, however, do not involve the effects of dynamic rupture propagation.

Dynamic Stress Drop

If we impose a non-negative condition on static stress drops by adjusting all negative values to be zero and by reducing their positive values to 90%, we obtain the stress-drop distribution as shown in Figure 7. These could be regarded as the dynamic stress drops constrained under these conditions. This model is called here the "non-negative stress-drop model" or model I. Figure 7 also gives the distribution of final slips calculated from the constrained stress drops and of strength excess. Figure 8 shows the distribution of dynamic slip, dynamic stress drop, and strength excess, all of which have been obtained by the alternative approach using the nonlinear inversion technique described in the Estimate of Dynamic Stress Drop subsection. This is called the "negative stress-drop model" or model II.

The dynamic stress-drop distribution in the two models indicates generally similar but somewhat different features. The high slips located at 14 to 17 km along the strike at depths of 8 to 12 km (Fig. 4) result from large, local stress drop. Model I indicates the existence of a localized stress drop of higher than 120 bars, yielding a fault slip of more than 180 cm (Fig. 7), while model II provides almost the same amount of slip of 180 cm with a maximum dynamic stress drop of 145 bars (Fig. 8). Although there are some differences in their absolute values, there is no doubt that the dynamic stress drop in the high-slip zone reached 120 to 140 bars. High slips around 50 to 70 cm in a somewhat broad zone located at 1 to 11 km along the strike at depths of 8 to 12 km can be attributed to dynamic stress drops of 20 to 45 bars in both models I and II. The slip exceeding 50 cm near the left edge of the fault (Fig. 4) may be accounted for by local stress drop of 15 to 35 bars in the two models.

A major difference in the two models lies in the shallow portion of the fault. Figure 7 indicates the existence of a wide zone of zero stress drop, which comes from the constraints involved in model I. In contrast, model II gives negative stress drops with several to about −15 bars over the zone of low slips at shallow depths (Fig. 8). It is to be noted here that this pattern with negative stress drops is essentially similar to that of the static stress drops shown in Figure 6. The negative stress drops in model II yielded zero or very low slips at the shallow section, whereas the zero stress drops in model I provided dynamic slips reaching 20 to 40 cm there, which appears to be somewhat larger than those detected from the waveform inversion. If, however, the low slips derived from the inversion had some allowance to this order, model I could be an equally adequate model.

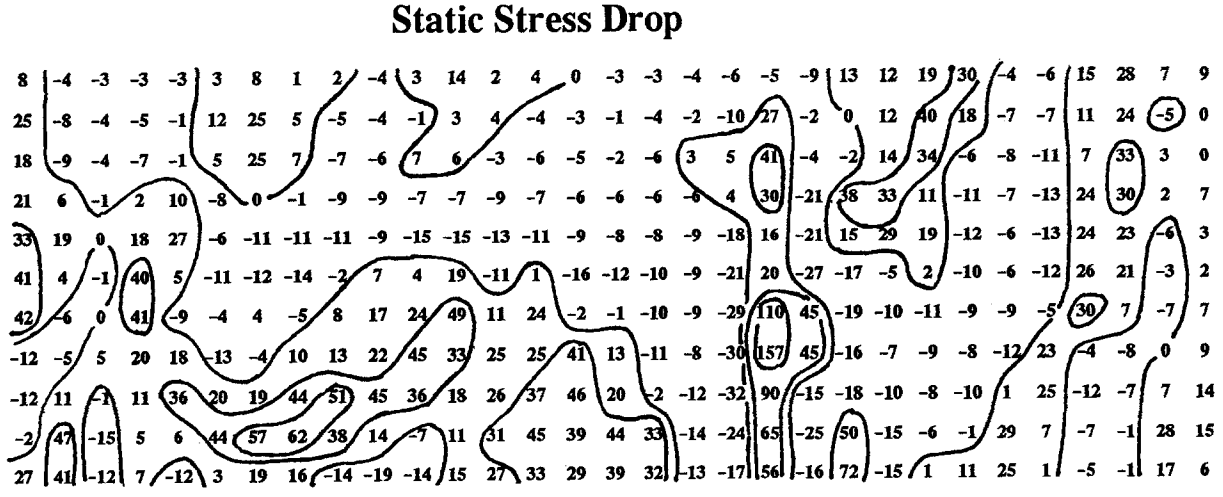

Figure 6. Distribution of the static stress drops recovered from the kinematic fault slips.

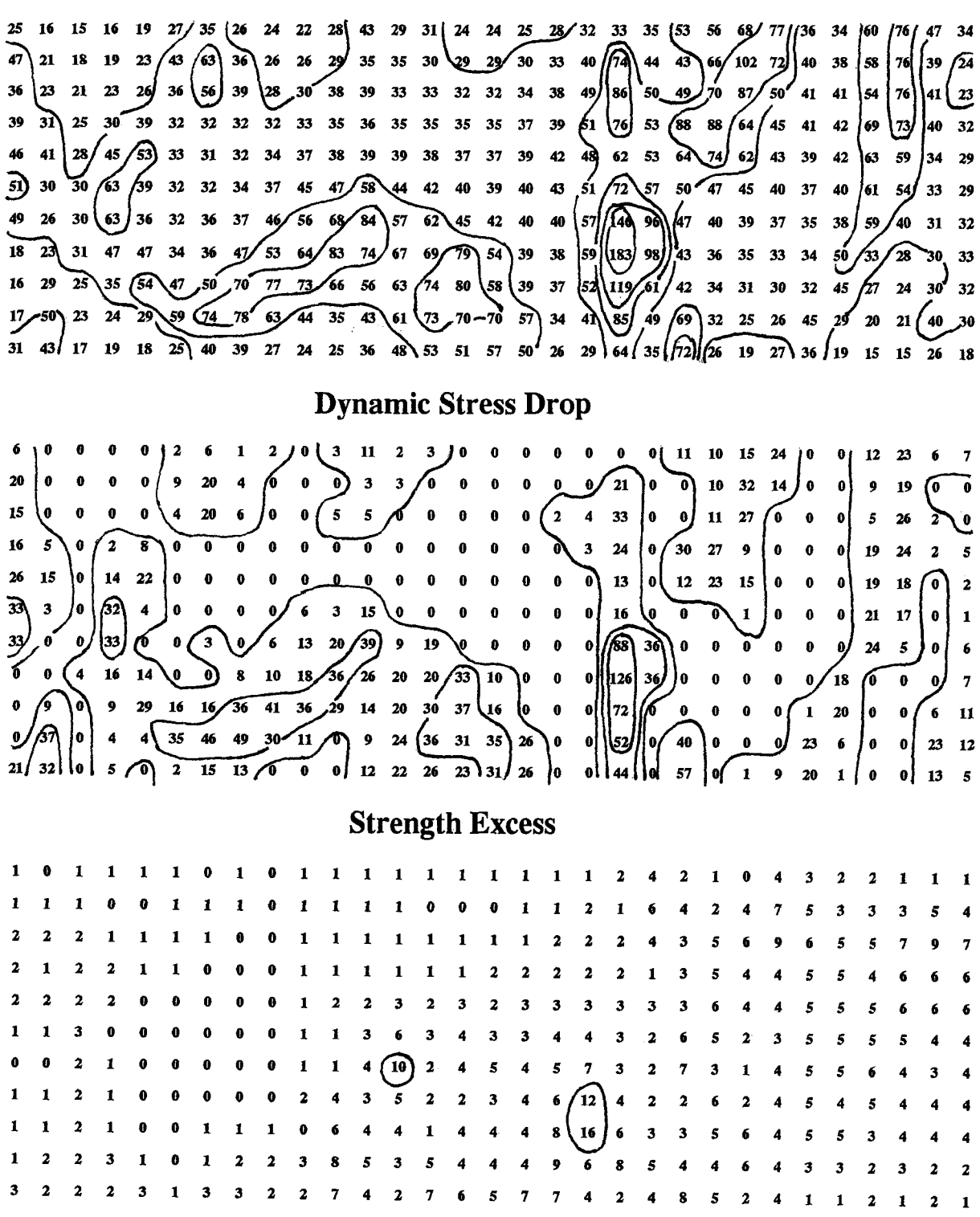

Figure 7. Distribution of the dynamic slip (in centimeters), dynamic stress drop (in bars), and strength excess (in bars) in model I (non-negative-stress-drop model) obtained from kinematic fault slips.

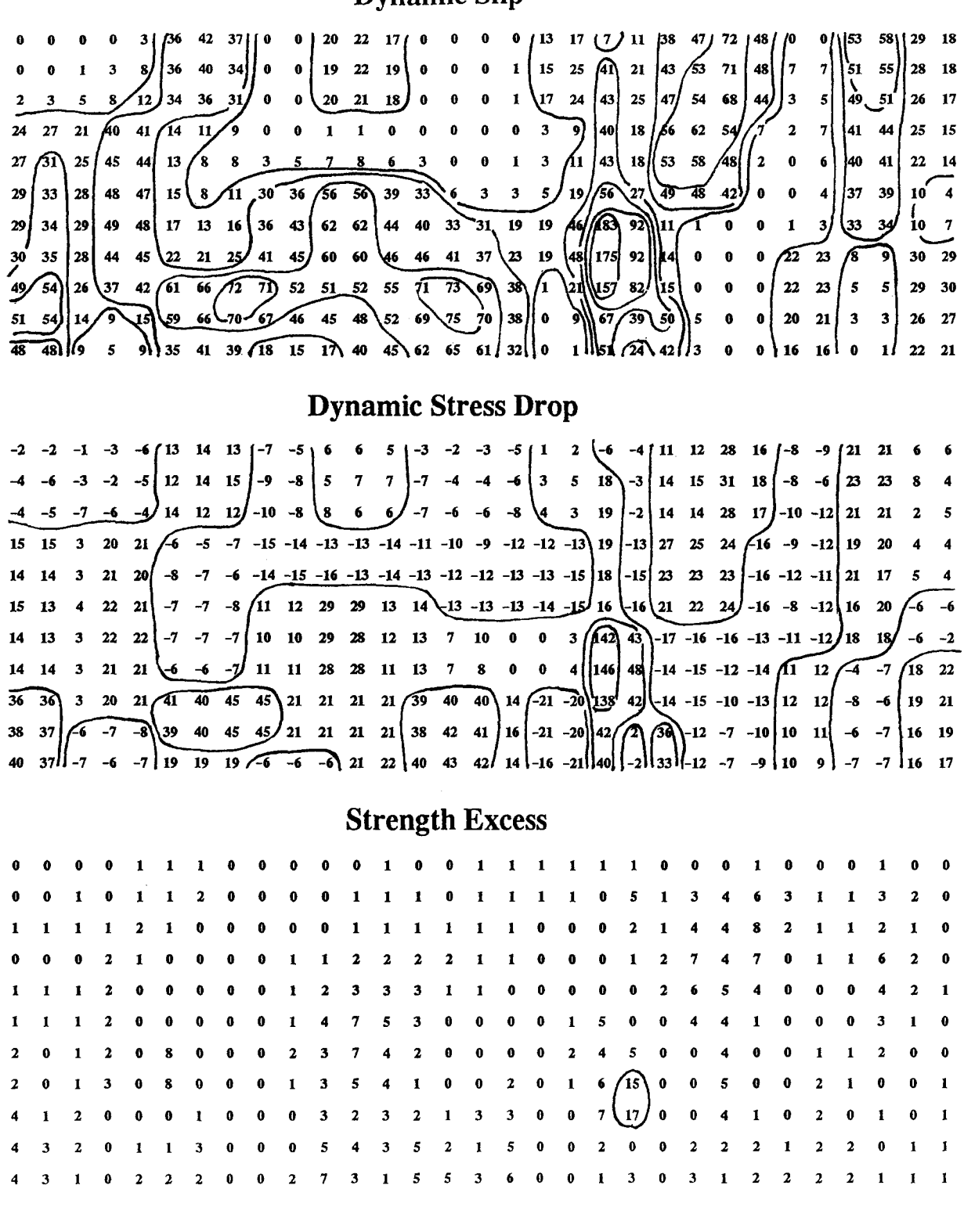

Figure 8. Distribution of the dynamic slip (in centimeters), dynamic stress drop (in bars), and strength excess (in bars) in model II (negative-stress-drop model) obtained from kinematic fault slips.

The total seismic moment calculated from models I and II is found to be 3.9×10^{25} and 2.7×10^{25} dyne cm, respectively, which are somewhat different from each other. Model II gives exactly the same moment as the kinematic fault model of Beroza and Spudich (1988). The larger moment in model I results from somewhat larger dynamic slips in the shallow fault section.

Strength Excess

There are no significant differences in the distribution of strength excess between the two results, as shown in Figures 7 and 8. This can be accounted for by the same technique applied to the two rupture models. The estimated strength excesses are generally small, although they are only the lower bounds, suggesting that the tectonic shear stress had reached close to the level of the fault strength before the earthquake over a major portion of the fault. The only exception is a moderate strength of about 15 bars on the fault segment located 14 to 17 km southeast away from the hypocenter at depths between 8 and 12 km. This segment corresponds to that of the delayed rupture (Fig. 4) and also to that of high dynamic stress drop. Beroza and Spudich (1988) have suggested that the segment near the Anderson Reservoir has either complex left-lateral offset or bending to the right, and that the rupture front was temporarily arrested here.

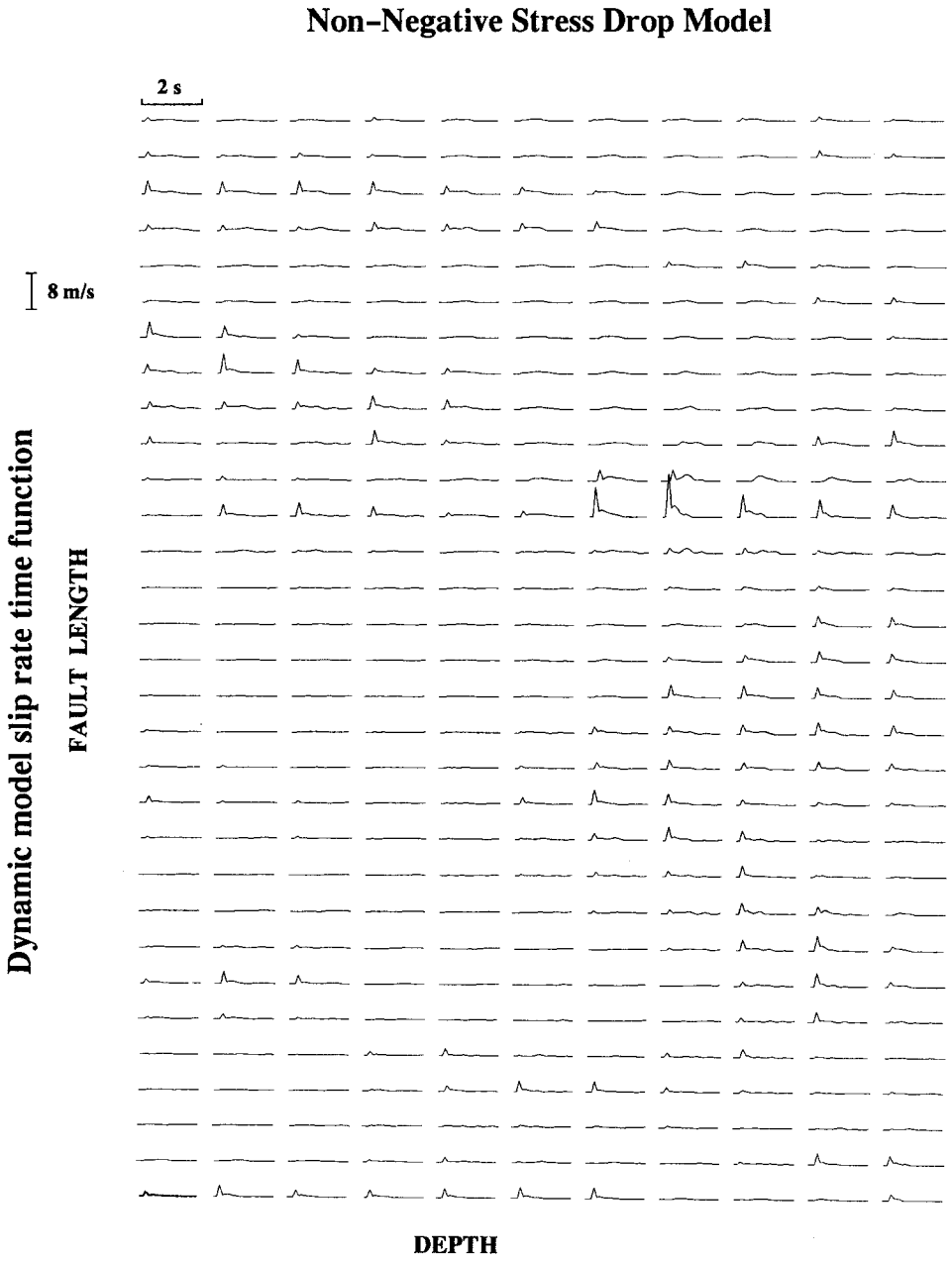

Figure 9. Distribution of the slip-rate functions on the fault in model I.

The present results suggest that the fault segment there may have a relative strength of more than 15 bars to be overcome, and that high stress drop occurred there. This could be called a moderate-strength asperity.

Slip-Velocity Source Time Function

Figures 9 and 10 show the dynamic slip-rate functions calculated from models I and II at every grid point on the fault plane. The origin time of these traces is taken at the rupture starting times at these points. It can be seen that the calculated slip-rate functions have a form of nearly an inverse square-root time dependence, and that the peak slip velocity varies remarkably with the location on the fault. The source functions appear to have rise times ranging between 0.2 and 0.5 sec, but the major portion with high slip rates is confined within the initial 0.2 to 0.3-sec time interval, although followed by a decaying tail at several high-velocity points. For the kinematic fault models, Hartzell and Heaton (1986) and Beroza and Spudich (1988) assumed the rise time of the source function to be 0.3 and 0.2 sec, respectively, being constant over the fault. Although dynamic rupture models generally yield rise times varying with the location on the fault and depending on the distribution of dynamic stress drop and fault strength, it is worth noting that the

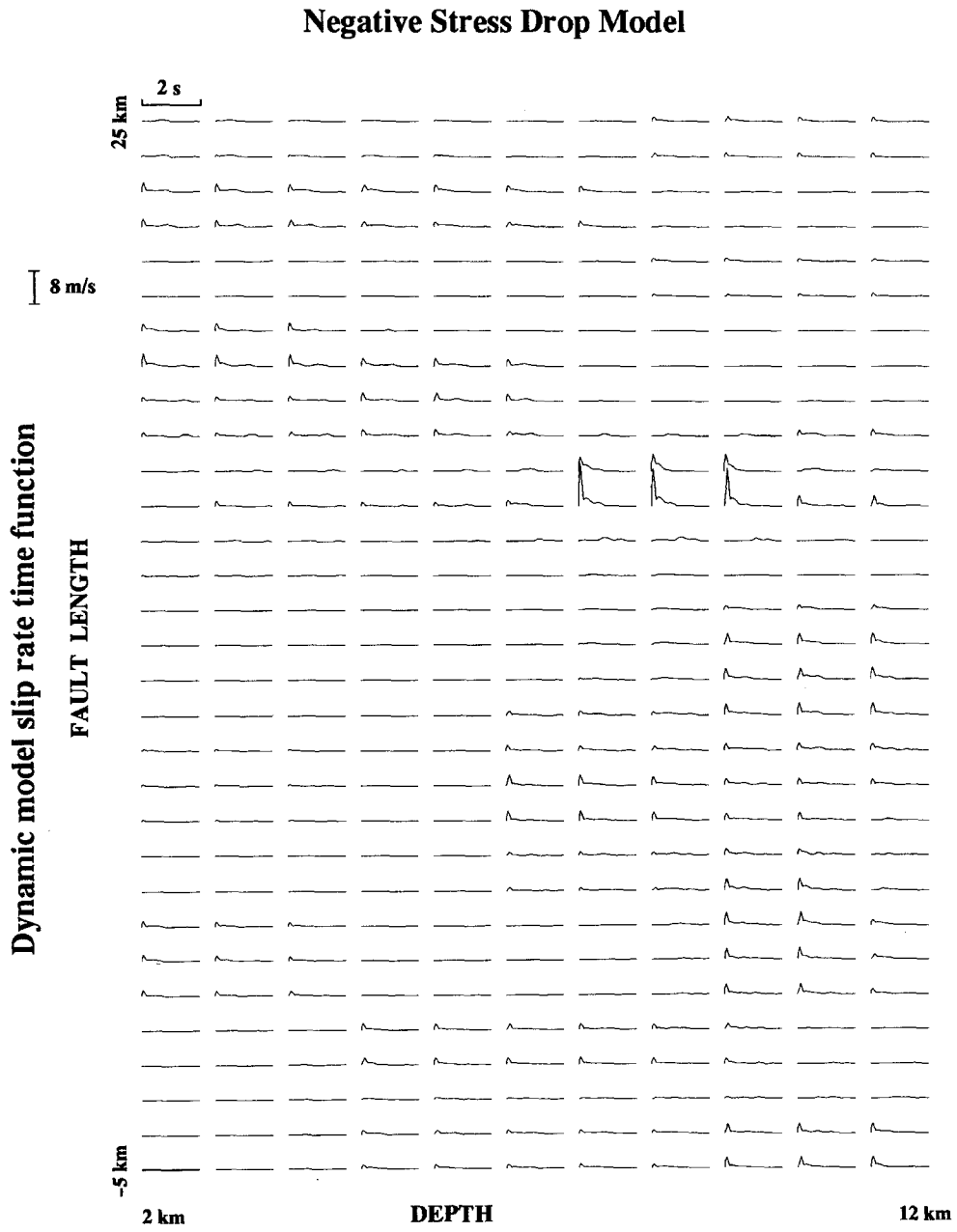

Figure 10. Distribution of the slip-rate functions on the fault in model II.

rise time for the major portion of the source function shown here is quite close to that assumed in the kinematic models. It is not necessarily clear at this moment, however, to what extent the calculated source time functions could reproduce the recorded waveforms. The synthetic seismograms to be compared with the recorded waveforms are being calculated and will be discussed in a companion article (Beroza and Mikumo, in preparation), and no such attempts have been made in the present article. Another possible way to solve this problem would be to perform kinematic waveform inversion and crack inversion alternately, as has been done in a recent article (Fukuyama and Mikumo, 1993).

Comparing Figure 9 with Figure 10, model II gives slightly larger slip rates and shorter rise times than model I. The difference may be due to the contrast between the larger and smaller (or negative) dynamic stress drops on the higher- and lower-slip zones. The maximum slip rate in the two models exceeds 8 m/sec in the zone of high stress drop, and appears to be comparable to that in the kinematic model.

Dynamic Rupture Propagation

Figures 11 and 12 illustrate a perspective view of dynamic rupture propagation and fault slips at time steps of every 1 sec in models I and II, respectively. The dynamic rupture initiated with a small stress drop at a nucleation zone (hypocenter) where the tectonic stress had reached the fault strength, then propagated southeast-

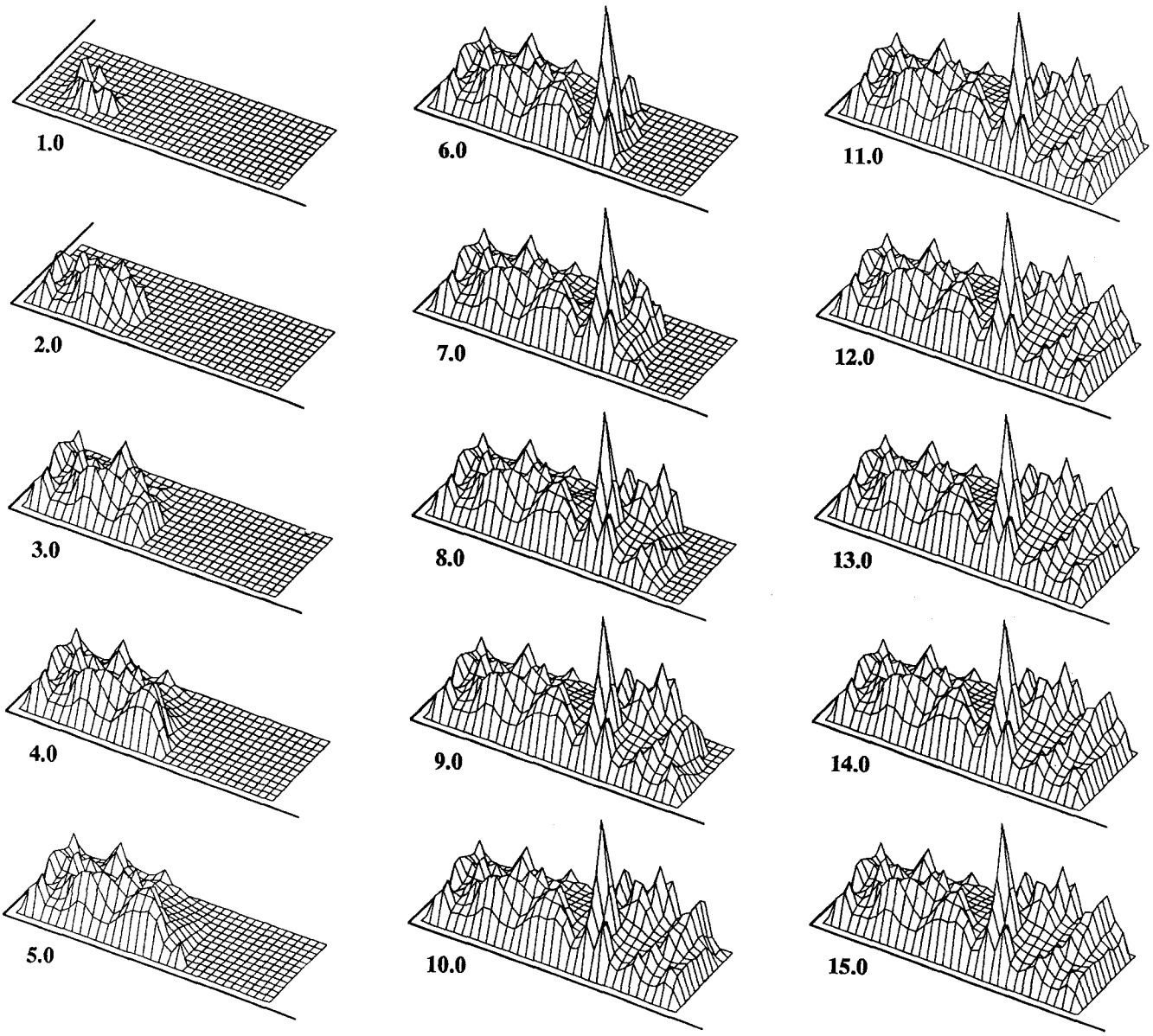

Figure 11. A perspective view of dynamic rupture propagation (seconds) and fault slips in model I. The height on the figures is proportional to slip amplitude.

ward, breaking the deeper section of the fault with high stress drops of 20 to 45 bars, by 5 sec after the initiation of the rupture. The rupture encountered the zones of very low or negative stress drop located at deeper and shallower fault sections. After a short time of arrest due to a relatively high-strength zone, the rupture broke this zone with a highest stress drop of more than 140 bars, yielding large slips exceeding 180 cm, and further propagated southeastward to the edge of the fault. The rupture yielded small slips even at the zones of negative or zero stress drop, as shown in Figures 7 and 8. The pattern of rupture propagation and the distribution of fault slip appear quite similar in models I and II, although the latter model gives somewhat smoother slip distribution.

Discussion

The present results suggest that there could be the zones of negative stress drop in the shallow portion of the crust between 3 and 8 km, if we refer to model II or the static model, although the fault slip at this depth might not be well resolved in the kinematic models.

Dynamic stress drop could be negative in the semi-brittle and ductile zones of the mid to lower crust (e.g., Tse and Rice, 1986), if the frictional sliding behavior changes from velocity weakening to velocity strengthening at temperatures above 300°C to 350°C, as has been suggested by recent laboratory experiments (e.g., Stesky, 1978; Blanpied *et al.*, 1991). In this case, however, neg-

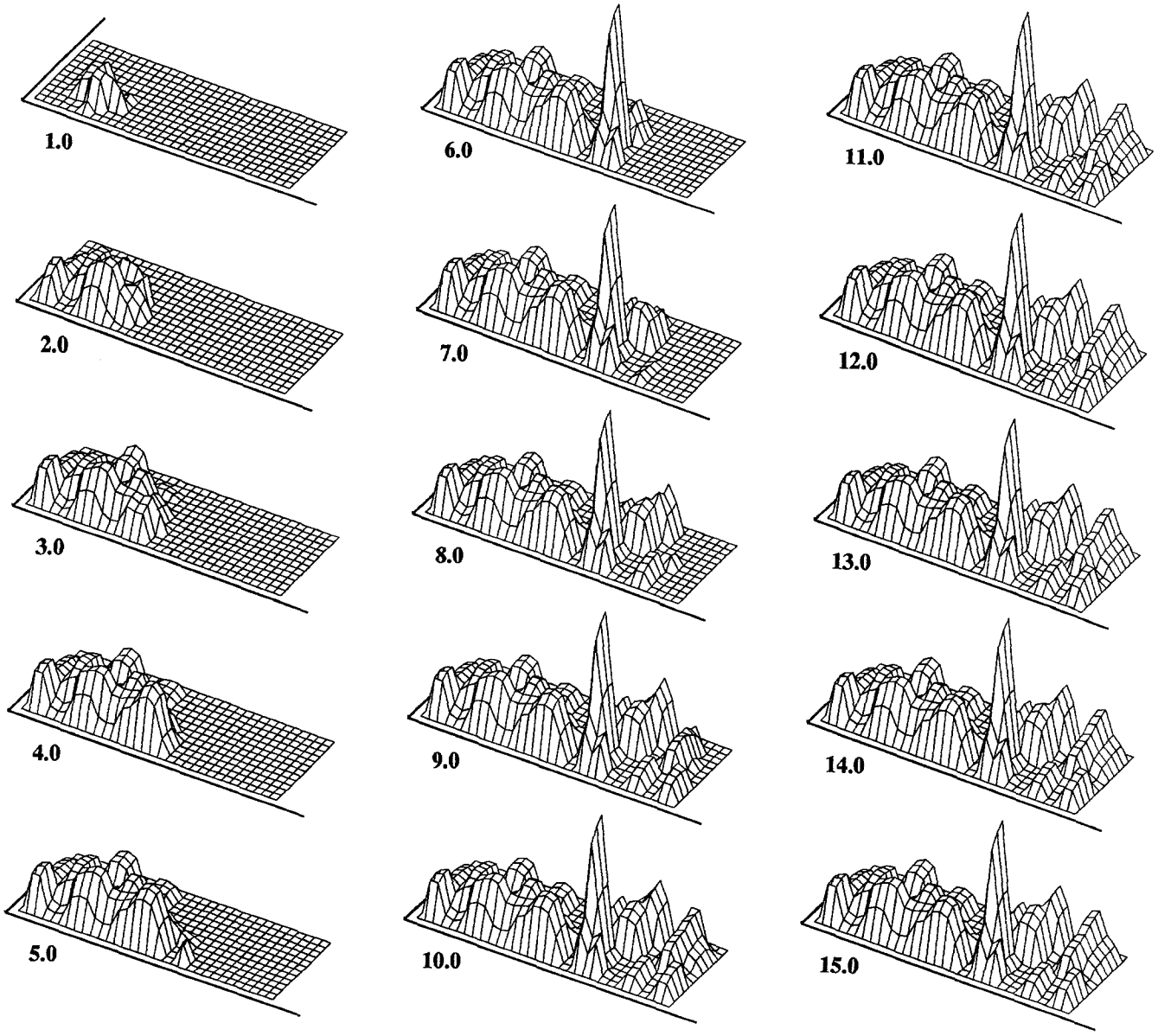

Figure 12. A perspective view of dynamic rupture propagation (seconds) and fault slips in model II. The height on the figures is proportional to slip amplitude.

ative stress drop would be expected in the semi-brittle zone at depths probably deeper than 8 km, depending on the temperature distribution within the crust (Mikumo, 1992). It has also been suggested that there might be a zone of velocity strengthening or negative stress drop in a very shallow part of the crust, i.e., in the sedimentary layers (Marone and Scholz, 1988; Scholz, 1990), where a thick unconsolidated fault gouge is likely to be present. The velocity strengthening would act to arrest large seismic slip (Marone and Scholz, 1988). This mechanism would be the case at depths shallower than 2 to 3 km, but unlikely to occur down to depths between 3 and 8 km as revealed in the present case.

Similar results have been obtained for the 1979 Imperial Valley, California, earthquake (Quin, 1990). Negative stress drops have been detected at depths shallower than 6 to 7 km over the entire fault and deeper than 13 km, although Miyatake's dynamic model for this earthquake (1992a) does not necessarily require negative stress drop to account for low slip at this depth range. Quin (1990) suggested that the negative stress drop at the shallow depths might be due to velocity strengthening in unconsolidated fault-gouge materials, although less emphasis was laid in this portion because of poor constraints on fault slips in the kinematic model and less accuracy of his dynamic model near the free surface. The present results in model II suggest more laterally heterogeneous, negative stress drops sandwiched between positive-stress-drop zones. A common feature in the two California earthquakes is the possible existence of negative-stress-drop zones at depths of 3 to 7 km, which might be characteristic at this depth range along strike-slip California faults.

One possible explanation would be that there could be patched zones of high temperature or unconsolidated fault gouge even at this depth, which yields velocity-strengthening frictional behavior and hence arrests large slip during dynamic rupture of the mainshock. It should also be noted that many aftershocks of the 1984 Morgan Hill earthquake were distributed, as reproduced in Fig-

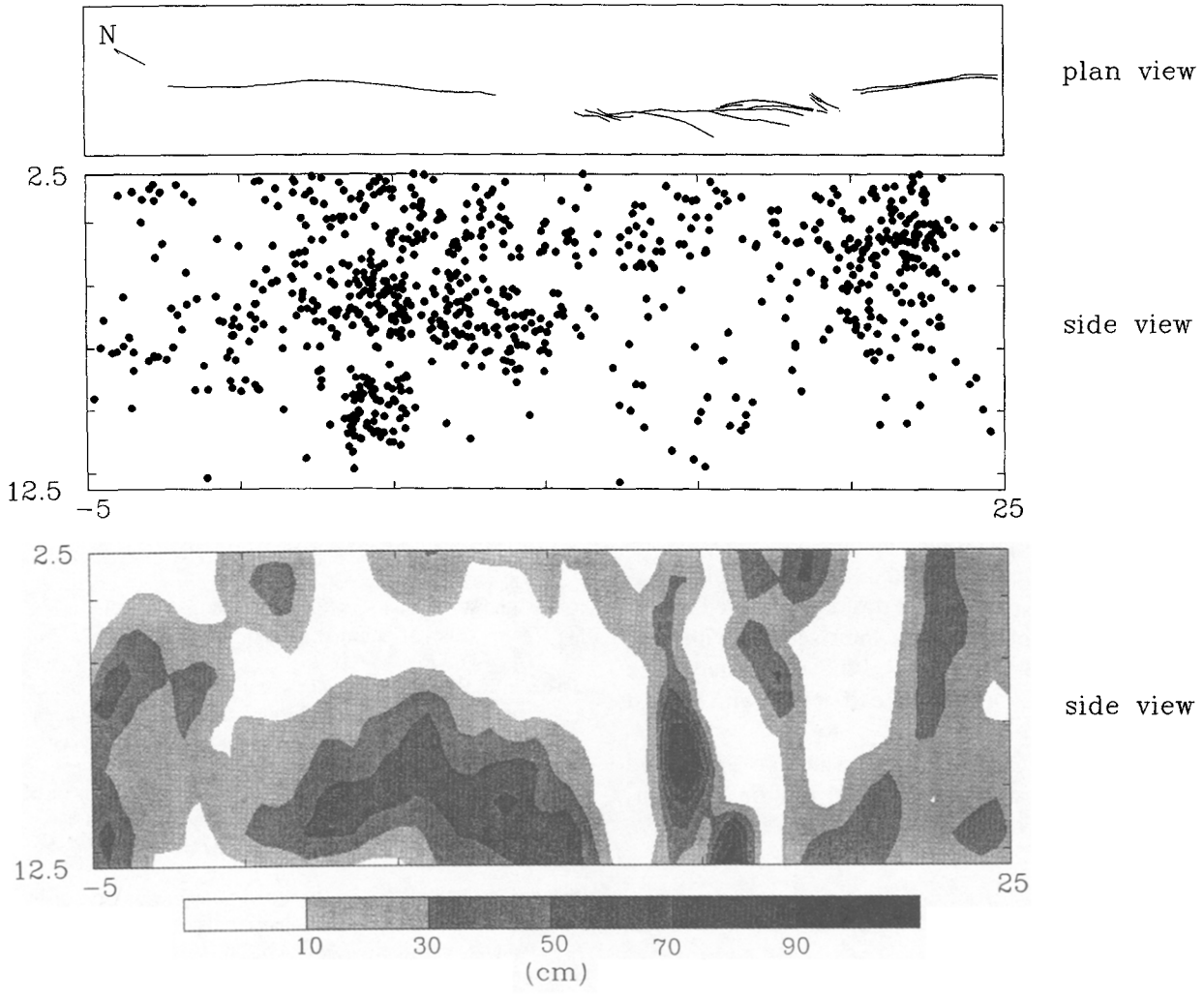

Figure 13. Side views of aftershock distribution and slip distribution, projected onto the fault plane (after Beroza and Spudich, 1988).

ure 13 (Cockerham and Eaton, 1987; Beroza and Spudich, 1988), over the low-slip or negative-stress-drop zones but not on the high-stress-drop zones. These features may be accounted for by the postseismic increase of the shear stress in the negative-stress-drop zones and the release of the stress in the high-stress-drop zones after the mainshock.

Conclusions

Our main purpose in this study was to derive the spatial distribution of dynamic stress drop and relative fault strength from the distribution of fault slip and rupture times obtained from a previous waveform inversion (Beroza and Spudich, 1988). For this purpose, a fracture criterion is introduced into a 3D dynamic rupture model, under which dynamic rupture propagation remains locked at each segment until the time specified from the waveform inversion. A lower bound of the peak shear stress just before rupturing this segment and hence of the strength excess or the relative fault strength has been estimated. Under these constraints, the distribution of static and dynamic stress drops has also been evaluated independently, by linear and nonlinear inversion procedures, respectively, from that of the kinematic fault slips derived from the waveform inversion.

The main conclusions obtained here are summarized as follows.

1. The large slips extending from the hypocenter to about 10 km and between 14 and 17 km along the strike at depths of 8 to 12 km come from local dynamic stress drop higher than 40 and 140 bars, respectively.
2. Negative stress drops down to -15 bars are required to account for very low slips over a shallow fault section, suggesting that there could be a zone of velocity-strengthening behavior there.
3. The strength excess is found to be generally small, but somewhat larger at a small section that has delayed rupture propagation.
4. The dynamic rupture initiated from a small nucleation zone with a low stress drop, propagated southeastward, breaking a deeper fault section with high stress drop, and finally broke the moderately high strength zone after a short time of arrest, with highest stress drop.
5. The aftershocks were distributed mainly on and around the negative-stress-drop zones but few on the high-stress-drop zones.

Acknowledgments

We are grateful to Dr. Greg Beroza for providing us the calculated results involved in Beroza and Spudich (1988) and many valuable comments on the draft of the present article. We also wish to thank Drs. Chuck Ammon and Grant Lindley and an anonymous reviewer for the improvement of the manuscript. The calculations involved here were made on a Cray computer at UNAM and also on a SUN-Spark II at CENAPRED, Mexico.

References

Andrews, D. J. (1976). Rupture velocity of plane strain shear cracks, *J. Geophys. Res.* **81**, 5679–5687.

Bakun, W. H., M. M. Clark, R. S. Cockerham, W. L. Ellsworth, A. G. Lindh, W. H. Prescott, A. F. Shakal, and P. Spudich (1984). The Morgan Hill, California, earthquake, *Science* **225**, 288–291.

Beroza, G. C. and P. Spudich (1988). Linearized inversion for fault rupture behavior: application for the 1984 Morgan Hill, California, earthquake, *J. Geophys. Res.* **93**, 6275–6296.

Blanpied, M. L., D. A. Lockner, and J. D. Byerlee (1991). Fault stability inferred from granite sliding experiments at hydrothermal conditions, *Geophys. Res. Lett.* **18**, 609–612.

Bluming, P., W. D. Mooney, and W. H. K. Lee (1985). Crustal structure of the southern Calaveras fault zone, central California, from seismic refraction investigations, *Bull. Seism. Soc. Am.* **75**, 193–209.

Boatwright, J. and H. Quin (1986). The seismic radiation from a 3-D dynamic model of a complex rupture process. Part I: confined ruptures, in *Earthquake Source Mechanics*, edited by S. Das, J. Boatwright, and C. Scholz (Editors), American Geophysical Union, Washington, D.C. 97–109.

Brady, A. G., R. L. Porcella, G. N. Boycroft, E. C. Etheredge, P. N. Mork, B. Silverstein, and A. F. Shakal (1984). The Morgan Hill, California, earthquake of April 24, 1984, *U.S. Geol. Surv. Open-File Rept. 84-498B.*

Cockerham, R. S. and J. P. Eaton (1987): "The earthquake and its aftershocks, April 24 through September 30, 1984," and "The Morgan Hill, California earthquake of April 24, 1984," *U.S. Geol. Surv. Bull.* **1639**, 15–28.

Das, S. (1981). Three-dimensional spontaneous rupture propagation and implication for the earthquake source mechanism, *Geophys. J. R. Astr. Soc.* **67**, 375–393.

Das, S. and K. Aki (1977). A numerical study of two-dimensional spontaneous rupture propagation, *Geophys. J. R. Astr. Soc.* **50**, 643–668.

Das, S. and B. V. Kostrov (1990). Inversion of seismic slip rate history and distribution with stabilizing constraints: application to the 1986 Andreanof Islands earthquake, *J. Geophys. Res.* **95**, 6899–6913.

Day, S. M. (1982). Three-dimensional simulation of spontaneous rupture: the effect of nonuniform prestress, *Bull. Seism. Soc. Am.* **72**, 1881–1902.

Ellsworth, W. L. and S. M. Marks (1980). Seismicity of the Livermore Valley, California, region, 1969–1979, *U.S. Geol. Surv. Open-File Rept. 84-515.*

Fukuyama, E. (1991a). Analysis and interpretation of the heterogenous rupture process: application of the empirical Green's function method and nonlinear inversion technique to large earthquakes, *Tectonophysics* **197**, 1–17.

Fukuyama, E. (1991b). Inversion for the rupture details of the 1987 east Chiba earthquake, Japan, using a fault model based on the distribution of relocated aftershocks, *J. Geophys. Res.* **96**, 8205–8217.

Fukuyama, E. and K. Irikura (1986). Rupture process of the 1983 Japan Sea (Akita-Oki) earthquake using a waveform inversion method, *Bull. Seism. Soc. Am.* **76**, 1623–1649.

Fukuyama, E. and T. Mikumo (1993). Dynamic rupture analysis: inversion for the source process of the 1990 Izu-Oshima, Japan earthquake (M6.5), *J. Geophys. Res.* **98**, 491–496.

Hartzell, S. (1989). Comparison of seismic waveform inversion re-

sults for the rupture history of a finite fault: application to the 1986 North Palm Springs, California, earthquake, *J. Geophys. Res.* **94**, 7515–7534.

Hartzell, S. H. and T. H. Heaton (1983). Inversion of strong motion and teleseismic waveform data for the fault rupture history of the 1979 Imperial Valley, California earthquake, *Bull. Seism. Soc. Am.* **73**, 1553–1583.

Hartzell, S. H. and T. H. Heaton (1986). Rupture history of the 1984 Morgan Hill, California, earthquake, from the inversion of strong motion records, *Bull. Seism. Soc. Am.* **76**, 649–674.

Hartzell, S. and M. Iida (1990). Source complexity of the 1987 Whittier Narrows, California, earthquake from the inversion of strong motion records, *J. Geophys. Res.* **95**, 12475–12485.

Hartzell, S. H., G. S. Stewart, and C. Mendoza (1991). Comparison of L1 and L2 norms in a teleseismic waveform inversion for the slip history of the Loma Prieta, California, earthquake, *Bull. Seism. Soc. Am.* **81**, 1518–1539.

Kikuchi, M. and H. Kanamori (1982). Inversion of complex body waves, *Bull. Seism. Soc. Am.* **72**, 491–506.

Kikuchi, M. and H. Kanamori (1991). Inversion of complex body waves—III, *Bull. Seism. Soc. Am.* **81**, 2335–2350.

Kikuchi, M. and Y. Fukao (1985). Iterative deconvolution of complex body waves from great earthquakes: the Tokachi-Oki earthquake of 1968, *Phys. Earth Planet. Interiors* **37**, 235–248.

Liu, H. L. and D. V. Helmberger (1983). The near-source ground motion of the 6 August 1979 Coyote Lake, California, earthquake, *Bull. Seism. Soc. Am.* **73**, 201–218.

Marone, C. and C. H. Scholz (1988). The depth of seismic faulting and the upper transition from stable to unstable slip regions, *Geophys. Res. Lett.* **15**, 621–624.

Mendoza, C. and S. Hartzell (1988). Aftershock patterns and main-shock faulting, *Bull. Seism. Soc. Am.* **78**, 1438–1449.

Mendoza, C. and S. Hartzell (1989). Slip distribution of the 19 September 1985 Michoacan, Mexico, earthquake: near-source and teleseismic constraints, *Bull. Seism. Soc. Am.* **79**, 655–669.

Mikumo, T. (1992). Dynamic fault rupture and stress recovery processes in continental crust under depth-dependent shear strength and frictional parameters, *Tectonophysics* **211**, 201–222.

Mikumo, T. and T. Miyatake (1978). Dynamical rupture process on a three-dimensional frictional fault with non-uniform frictions and near-field seismic waves, *Geophys. J. R. Astr. Soc.* **54**, 417–438.

Mikumo, T., K. Hirahara, and T. Miyatake (1987). Dynamic fault rupture processes in heterogeneous media, *Tectonophysics* **144**, 19–36.

Mikumo, T. and T. Miyatake (1993). Dynamic rupture processes on a dipping fault, and estimates of stress drop and strength excess from the results of waveform inversion, *Geophys. J. Int.* **112**, 481–496.

Miyatake, T. (1980). Numerical simulations of earthquake source process by a three-dimensional crack model. Part I. Rupture process, *J. Phys. Earth* **28**, 565–598.

Miyatake, T. (1992a). Reconstruction of dynamic rupture process of an earthquake with constraints of kinematic parameters, *Geophys. Res. Lett.* **19**, 349–352.

Miyatake, T. (1992b). Dynamic rupture processes of inland earthquakes in Japan: weak and strong asperities, *Geophys. Res. Lett.* **19**, 1041–1044.

Olson, A. H. and R. Apsel (1982). Finite faults and inverse theory with applications to the 1979 Imperial Valley earthquake, *Bull. Seism. Soc. Am.* **72**, 1969–2002.

Quin, H. (1990). Dynamic stress drop and rupture dynamics of the October 15, 1979 Imperial Valley, California earthquake, *Tectonophysics* **175**, 93–117.

Scholz, C. H. (1990). *The Mechanics of Earthquakes and Faulting*, Cambridge Univ. Press, Cambridge.

Shakal, A. F., R. W. Sherburne, and D. L. Parke (1984). CDMG strong motion records from the Morgan Hill, California, earthquake of 24 April 1984, Rept. 84-7, Office of Strong Motion Studies, Sacramento, California.

Spudich, P. and L. N. Frazier (1984). Use of ray theory to calculate high-frequency radiation from earthquake sources having spatially variable rupture velocity and stress drop, *Bull. Seism. Soc. Am.* **74**, 2061–2082.

Steidl, J. H., R. J. Archuleta, and S. H. Hartzell (1991). Rupture history of the 1989 Loma Prieta, California, earthquake, *Bull. Seism. Soc. Am.* **81**, 1573–1602.

Stesky, R. M. (1978). Mechanism of high temperature frictional sliding in Westerly granite, *Can. J. Earth Sci.* **15**, 361–375.

Takeo, M. (1987). An inversion method to analyze the rupture process of earthquakes using near-field seismograms, *Bull. Seism. Soc. Am.* **77**, 490–513.

Takeo, M. (1988). Rupture process of the 1980 Izu-Hanto-Oki earthquake deduced from strong motion seismograms, *Bull. Seism. Soc. Am.* **78**, 1074–1091.

Takeo, M. and N. Mikami (1987). Inversion of strong motion seismograms for the source process of the Nagano-Ken-Seibu earthquake of 1984, *Tectonophysics* **144**, 271–285.

Takeo, M. and N. Mikami (1990). Fault heterogeneity of inland earthquakes in Japan, *Bull. Earthquake Res. Inst.* **65**, 541–569.

Tse, S. T. and J. R. Rice (1986). Crustal earthquake instability in relation to the depth variation of frictional slip properties, *J. Geophys. Res.* **91**, 9452–9472.

Virieux, J. and R. Madariaga (1982). Dynamic faulting studied by a finite difference method, *Bull. Seism. Soc. Am.* **72**, 345–369.

Wald, D. J., D. V. Helmberger, and S. H. Hartzell (1990). Rupture process of the 1987 Superstitions Hills earthquake from the inversion of strong motion data, *Bull. Seism. Soc. Am.* **80**, 1079–1098.

Wald, D. J., D. V. Helmberger, and T. H. Heaton (1991). Rupture model of the 1989 Loma Prieta earthquake from the inversion of strong-motion and broadband teleseismic data, *Bull. Seism. Soc. Am.* **81**, 1540–1572.

Yoshida, S. (1986). A method of waveform inversion for earthquake rupture process, *J. Phys. Earth* **34**, 235–255.

Zeng, Y., K. Aki, and T. L. Teng (1993). Source inversion of the 1987 Whittier Narrows earthquake, California, using the isochron method, *Bull. Seism. Soc. Am.* **83**, 358–377.

Centro Nacional de Prevencion de Desastres
Mexico 04360 D. F., Mexico
(T. Mikumo)

Earthquake Research Institute
University of Tokyo
Tokyo 113, Japan
(T. Miyatake)

Manuscript received 3 August 1993.